Journal of Sound and Vibration (2000) **235**(5), 727–747
doi:10.1006/jsvi.2000.2978, available online at http://www.idealibrary.com on IDEAL®

VIBRATION OF STIFFENED PLATES USING HIERARCHICAL TRIGONOMETRIC FUNCTIONS

MICHEL BARRETTE, ALAIN BERRY AND OLIVIER BESLIN

GAUS, Department of mechanical engineering, University of Sherbrooke, Sherbrooke (Qc) Canada J1K 2R1

(*Received* 26 *August* 1999, *and in final form* 25 *January* 2000)

The vibration analysis of stiffened plates using hierarchical finite elements with a set of local trigonometric interpolation functions is presented. The local functions extend on the plate domain comprised between consecutive stiffeners, thereby allowing a coarse discretization of the global structure. Convergence studies as well as comparison of the present approach with the literature and experimental results are presented. The great numerical stability of the trigonometric functions and their readiness for symbolic manipulations make them potentially attractive for vibration and sound radiation analysis in the mid-frequency range.

1. INTRODUCTION

Stiffened plates form an important class of engineering structures and are frequently encountered in ship or aircraft structures; the structural acoustics of stiffened plates is thus of interest with respect to the dynamics/noise aspects of such structures. Unfortunately, exact analytical methods are usually limited to the first few vibration modes, while approximate statistical methods are confined to high frequency. This work addresses a new and computationally efficient method of solving the vibration of plates reinforced by an array of orthogonal stiffeners, which should allow the predictions to be extended towards the mid-frequency range.

The analysis of stiffened plate vibration has been the subject of numerous work, mainly using the Rayleigh–Ritz technique or the finite element method (FEM). Earlier work using the Rayleigh–Ritz technique includes publications by Wu *et al.* [1], Laura *et al.* [2], Bhat [3], Gutierrez *et al.* [4], who considered pure bending deformation of the plate and essentially bending and torsion deformation of the stiffeners; other authors, e.g., Liew *et al.* [5, 6], Xiang *et al.* [7], have refined the models by considering a Mindlin plate model, including rotary inertia and transverse shear, as well as bending, torsion and transverse shear deformations of the stiffeners; Berry *et al.* [8] also included in-plane deformation of the plate and extensional deformation of the stiffeners. Other geometries have also been considered such as stiffened skew plates [7] and stiffened sector plates [9]. The sound radiation of stiffened plates has been investigated by Mace [10–12], Mead [13] and others for infinite and periodically stiffened plates and by Berry *et al.* [14, 8] and others for finite plates. Most of these studies used polynomial trial functions defined on the whole domain of the stiffened plate. In some situations, e.g., when heavy stiffeners are considered, such global trial functions have difficulties in reconstructing rapid spatial changes of the vibration field close to the stiffeners [8]; this results in ill-conditioned systems and inaccurate prediction.

0022-460X/00/350727 + 21 $35.00/0

On the other hand, the FEM uses a discretization of the global structure and interpolation functions which are local in nature. However, model size limitations still restrict conventional FEM to low frequency. In order to overcome these limitations, alternatives to the conventional FEM have been proposed: Koko *et al.* [15] have developed the so-called "super-elements" to model the free vibration of stiffened plates; these super-elements allow a coarser mesh to be considered (at the expense of more complex interpolation functions), typically one or a few elements between adjacent stiffeners. Chen *et al.* [16] used a spline compound strip method where the plate is being divided into finite strips and splines are used as trial functions. Coté [17] has applied the *p*-version of the FEM to several structural acoustics problems, including the vibration of stiffened plates; in the *p*-version of the FEM, the mesh of the structure is fixed and the order of the polynomial interpolation functions is increased until convergence is reached. In terms of CPU and memory requirements, there is a clear benefit of using the *p*-FEM as compared to conventional FEM when reaching the mid-frequency range. Bardell [18] has developed a hierarchical FEM, for the free vibration of plates; a distinct advantage of the hierarchical FEM is that the system matrices for a given interpolation order can be used to form the matrices for a larger interpolation order. The interpolation functions used by Bardell are based on integrated Legendre orthogonal polynomials. Bardell used symbolic computing to calculate high order polynomial coefficients and matrix elements. These functions have been applied to the free vibration of periodically stiffened, infinite flat plates [19]; in this case, plate bays present between adjacent stiffeners formed single elements. Recently, Beslin *et al.* [20] have proposed a set of trigonometric hierarchical functions in order to predict high order modes of vibration of bending plates with arbitrary boundary conditions. The trigonometric set offers better numerical stability at higher frequency, as compared to the polynomial set of Bardell.

In this study, the hierarchical trigonometric functions of Beslin are used as local trial functions in the prediction of stiffened plate vibration. The local functions are defined on the plate domain present between consecutive stiffeners, thereby allowing a coarse discretization of the global structure. In addition to their simplicity and numerical stability, the trigonometric functions lend themselves to the use of exact, symbolic integration and lead to simple inter-element conditions at the stiffener locations. In the following, the theoretical formulation is detailed and numerical results are shown for both unstiffened and stiffened plates.

2. ENERGY EXPRESSIONS

We first consider a rectangular, flat, isotropic plate (referred to as a "plate element") of dimensions a, b, thickness h, subject to pure bending deformation. Figure 1 shows this plate element and the corresponding co-ordinate systems. Non-dimensional co-ordinates $\xi = (2/a)x - 1$, $\eta = (2/b)y - 1$ are used in the following, such that the plate element corresponds to $-1 \leqslant \xi \leqslant +1$ and $-1 \leqslant \eta \leqslant +1$.

The kinetic energy of the plate is given by

$$T_p = \frac{\rho ab}{8} \int_{-1}^{+1} \int_{-1}^{+1} w_{,t}^2 \, \mathrm{d}\xi \, \mathrm{d}\eta, \tag{1}$$

where $w(\xi, \eta)$ is the transverse displacement and ρ is the density of the plate material. The strain or bending energy of the plate is

$$V_p = \frac{2Db}{a^3} \int_{-1}^{+1} \int_{-1}^{+1} \left[w_{,\xi\xi}^2 + \left(\frac{a}{b}\right)^4 w_{,\eta\eta}^2 + 2\nu \left(\frac{a}{b}\right)^2 w_{,\xi\xi} w_{,\eta\eta} + 2(1-\nu)\left(\frac{a}{b}\right)^2 w_{,\xi\eta}^2 \right] \mathrm{d}\xi \, \mathrm{d}\eta, \tag{2}$$

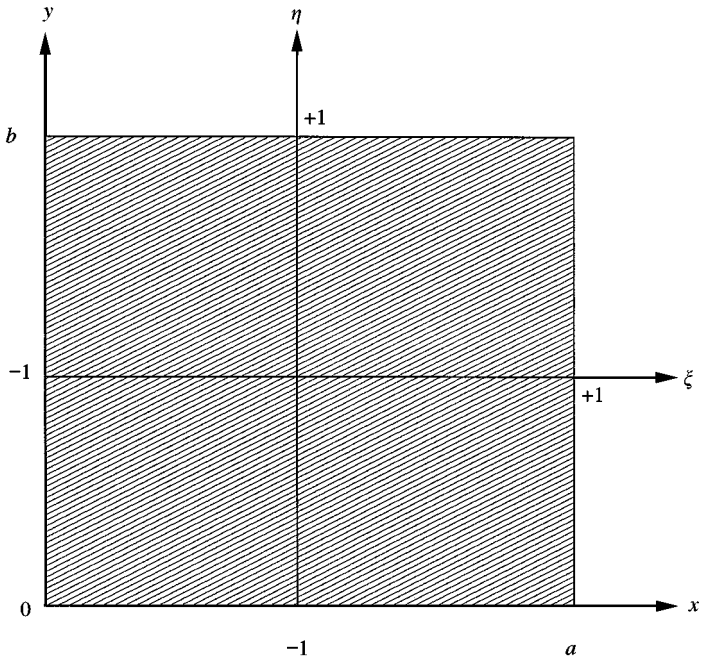

Figure 1. A plate element.

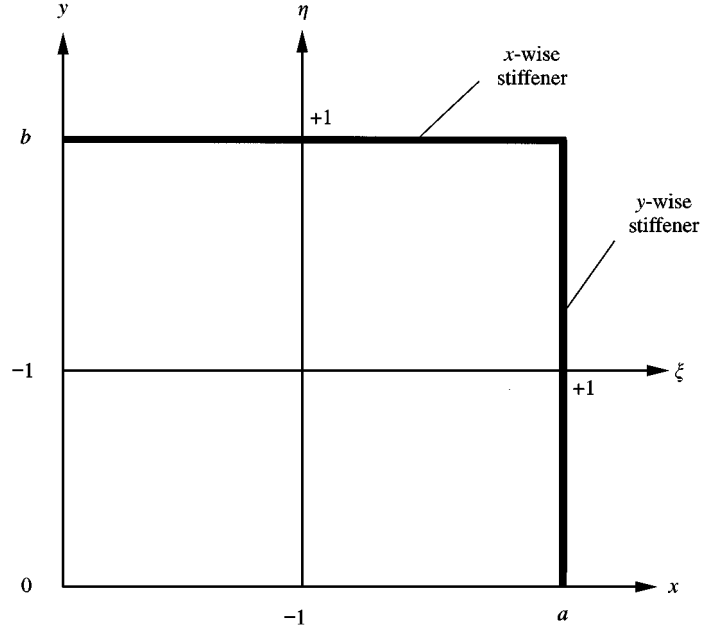

Figure 2. Stiffener elements.

where $D = Eh^3/(12(1 - \nu^2))$ is the bending stiffness and ν is the Poisson ratio of the plate.

We now consider two orthogonal, beam-like stiffeners attached to the plate at positions $x = a$ ("y-wise stiffener") and $y = b$ ("x-wise stiffener") (Figure 2). It is assumed that, as

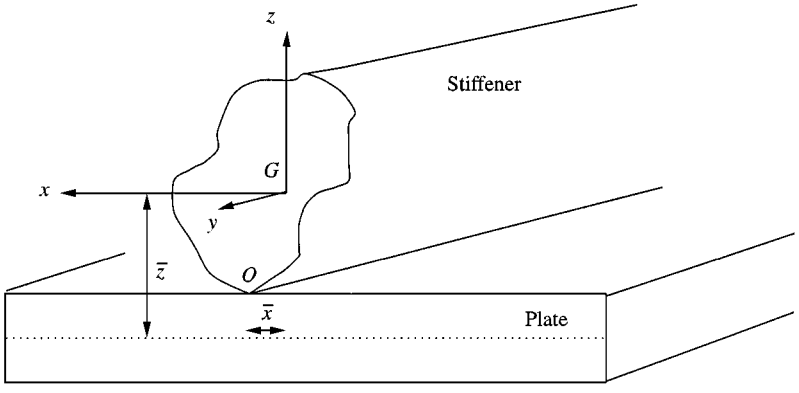

Figure 3. Stiffener geometric characteristics.

a result of the plate bending, the stiffeners are subject to bending and torsion deformations. Also, the attachment of the stiffeners to the plate is **lineic** and at each attachment point, the continuity of displacements and rotations is assumed between the plate and stiffener; therefore, all displacements and strains of the stiffeners can be expressed as a function of the plate displacement $w(\xi, \eta)$. Details on the displacements, strains and energy expressions regarding the stiffeners can be found in reference [14].

The kinetic energy of the y-wise stiffener is given by

$$T_y = \frac{\rho_y S_y b}{4}\int_{-1}^{+1}\left[w_{,t}^2(\xi_y,\eta) + \bar{z}^2\left(\frac{2}{a}\right)^2 w_{,\xi t}^2(\xi_y,\eta) + \bar{z}^2\left(\frac{2}{b}\right)^2 w_{,\eta t}^2(\xi_y,\eta)\right.$$
$$\left. + \bar{x}^2\left(\frac{2}{a}\right)^2 w_{,\xi t}^2(\xi_y,\eta) - \bar{x}\left(\frac{4}{a}\right) w_{,t}(\xi_y,\eta) w_{,\xi t}(\xi_y,\eta)\right]\mathrm{d}\eta$$
$$+ \frac{\rho_y I_{xx} b}{4}\int_{-1}^{+1}\left[\left(\frac{2}{a}\right)^2 w_{,\xi t}^2(\xi_y,\eta) + \left(\frac{2}{b}\right)^2 w_{,\eta t}^2(\xi_y,\eta)\right]\mathrm{d}\eta$$
$$+ \frac{\rho_y I_{zz} b}{4}\int_{-1}^{+1}\left(\frac{2}{a}\right)^2 w_{,\xi t}^2(\xi_y,\eta)\,\mathrm{d}\eta, \tag{3}$$

where ξ_y is the location of the y-wise stiffener. In our case (Figure 2), $\xi_y = 1$. Also, ρ_y is the density of the y-wise stiffener, S_y is the cross-section area, I_{xx} and I_{zz} are second moments of inertia with respect to the stiffener's center of inertia G, and $\bar{x}$ and $\bar{z}$ defined the position of the plate–stiffener junction O with respect to the stiffener's center of inertia (Figure 3).

The strain energy of the y-side stiffener is

$$V_y = \frac{4E_y(I_{xx} + S_y\bar{z}^2)}{b^3}\int_{-1}^{+1} w_{,\eta\eta}^2(\xi_y,\eta)\,\mathrm{d}\eta + \frac{4G_y J_y}{a^2 b}\int_{-1}^{+1} w_{,\xi\eta}^2(\xi_y,\eta)\,\mathrm{d}\eta, \tag{4}$$

where E_y is the Young's modulus, G_y is the shear modulus and J_y is the (Saint-Venant) torsion constant of the y-wise stiffener. The first term in the strain energy stands for the bending and the second term stands for the torsion of the stiffener. The kinetic energy T_x and strain energy V_x of the x-wise stiffener are obtained by permuting a and b, x and y as well as ξ and η in equations (3) and (4).

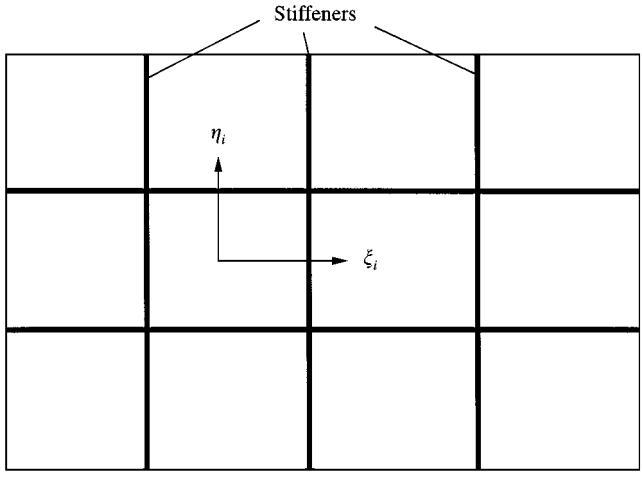

Figure 4. A plate with an array of orthogonal stiffeners.

The Hamilton functional of the plate–stiffeners system is

$$H = \int_{t_1}^{t_2} (T - V)\,\mathrm{d}t, \tag{5}$$

where $T = T_p + T_x + T_y$ and $V = V_p + V_x + V_y$.

Finally, let us consider a bending plate reinforced by an array of orthogonal stiffeners (Figure 4). Such a structure can be viewed as an assembly of plate elements with attached x-wise and y-wise stiffener elements, as considered previously. Local co-ordinates systems (x^i, y^i) and (ξ^i, η^i) are defined for each elements i.

Since the global structure is formed by assembling plate and stiffener elements, it is planar but its geometry is not necessarily rectangular; also, the array of stiffeners is not necessarily periodic as the dimensions of the elements may vary, and the plate and stiffener properties can vary from one element to an other. The boundary conditions along the sides of the plate elements that define the contour of the global plate can be taken as simply supported, clamped or free, and may vary from one plate element to another.

The Hamilton functional of the global structure is

$$H = \int_{t_1}^{t_2} (T - V)\,\mathrm{d}t, \tag{6}$$

where $T = \sum_i (T_p^i + T_x^i + T_y^i)$ and $V = \sum_i (V_p^i + V_x^i + V_y^i)$. The summation is done on all the plate elements and stiffeners of the global structure. The variational principle states that the free vibration of the global structure satisfies

$$\delta H = 0. \tag{7}$$

3. RAYLEIGH–RITZ METHOD

3.1. LOCAL TRIGONOMETRIC TRIAL FUNCTIONS

The local displacement field $w^i(\xi^i, \eta^i, t)$ on the element i is expressed as

$$w^i(\xi^i, \eta^i, t) = \sum_{m=1}^{M^i} \sum_{n=1}^{N^i} q_{mn}^i(t)\,\phi_m(\xi^i)\,\phi_n(\eta^i), \tag{8}$$

TABLE 1

Table of coefficients (a_m, b_m, c_m, d_m) *relative to the trigonometric set* $\phi_m(\xi)$ *where* $\phi_m(\xi) = \sin(a_m\xi + b_m)\sin(c_m\xi + d_m)$

m	a_m	b_m	c_m	d_m
1	$\pi/4$	$3\pi/4$	$\pi/4$	$3\pi/4$
2	$\pi/4$	$3\pi/4$	$\pi/2$	$3\pi/2$
3	$\pi/4$	$-3\pi/4$	$\pi/4$	$-3\pi/4$
4	$\pi/4$	$-3\pi/4$	$\pi/2$	$-3\pi/2$
>4	$\pi/2(m-4)$	$\pi/2(m-4)$	$\pi/2$	$\pi/2$

where $\phi_m(\xi^i)$ an $\phi_n(\eta^i)$ are trial functions, M^i and N^i are the numbers of functions along the x and y directions, and the q^i_{mn} are the local unknown Rayleigh–Ritz coefficients, defined on the element i. In this work, the trigonometric functions introduced by Beslin [20] are used as the trial functions.

The trigonometric set $\{\phi_m(\xi)\}$ is defined as

$$\phi_m(\xi) = \sin(a_m\xi + b_m)\sin(c_m\xi + d_m), \tag{9}$$

where coefficients a_m, b_m, c_m, d_m are given in Table 1. The functions ϕ_m are plotted in Figure 5. These function have useful properties, their shape, similar to the polynomial functions of Bardell allows arbitrary boundary conditions to be specified by selecting proper combinations among the first four functions. These functions also allow a simple assembly of plate elements as will be shown in section 4. The most attractive particularity of the trigonometric function is that they offer great numerical stability and, contrary to the polynomial functions, do not require special attention to the round-off errors. Beslin [20] showed that very high expansion orders can be used in equation (8) so that the medium frequency range can be approached with a reasonable number of trial functions.

3.2. ELEMENTARY MASS AND STIFFNESS MATRICES

Substituting equation (8) into equation (1), the kinetic energy of the plate element i is

$$T^i_p = (\dot{\mathbf{q}}^i)^{\mathrm{T}}\mathbf{M}^i_p\dot{\mathbf{q}}^i, \tag{10}$$

where $\dot{\mathbf{q}}^i = \{q^i_{mn,t}\}$ and $\mathbf{q}^i = \{q^i_{mn}\}$ is the vector of the Rayleigh–Ritz coefficients for the plate element i and $\mathbf{M}^i_p$ is the elementary mass matrix of the plate element i,

$$\mathbf{M}^i_p = [M^i_{pmnrs}] = \frac{\rho^i h^i a^i b^i}{4}[I^{00}_{mr} I^{00}_{ns}]. \tag{11}$$

Similarly, the strain energy of the plate element i is

$$V^i_p = (\mathbf{q}^i)^{\mathrm{T}}\mathbf{K}^i_p\mathbf{q}^i, \tag{12}$$

m	w		$w,\ \xi$		Plot
	$\xi=-1$	$\xi=1$	$\xi=-1$	$\xi=1$	
$m=1$	1	0	0	0	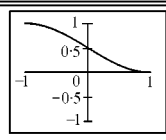
$m=2$	0	0	$\pi/2$	0	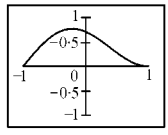
$m=3$	0	1	0	0	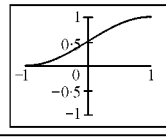
$m=4$	0	0	0	$\pi/2$	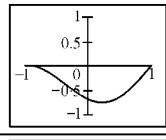
$m=5$	0	0	0	0	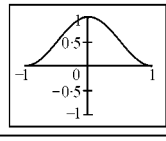
$m=6$	0	0	0	0	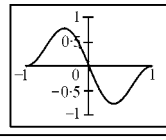
$m=7$	0	0	0	0	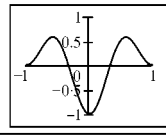
$m=8$	0	0	0	0	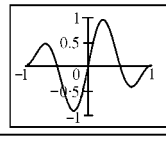
$m>8$	0	0	0	0	

Figure 5. Graphical representation of the first eight trigonometric functions. The value of the functions and their derivatives at the end points is reported.

where $\mathbf{K}_p^i$ is the elementary stiffness matrix of the plate element i,

$$\mathbf{K}_p^i = [K^i_{pmnrs}]$$

$$= \frac{4D^i b^i}{(a^i)^3}\left[I^{22}_{mr} I^{00}_{ns} + \left(\frac{a^i}{b^i}\right)^4 I^{00}_{mr} I^{22}_{ns} + v^i\left(\frac{a^i}{b^i}\right)^2 (I^{20}_{mr} I^{02}_{ns} + I^{02}_{mr} I^{20}_{ns})\right.$$

$$\left. + 2(1-v^i)\left(\frac{a^i}{b^i}\right)^2 I^{11}_{mr} I^{11}_{ns}\right]. \tag{13}$$

The terms $I_{mr}^{\alpha\beta}$ in equations (11) and (13) are defined by the integrals

$$I_{mr}^{\alpha\beta} = \int_{-1}^{+1} \frac{\mathrm{d}^{\alpha}\phi_m(\xi)}{\mathrm{d}\xi^{\alpha}} \frac{\mathrm{d}^{\beta}\phi_r(\xi)}{\mathrm{d}\xi^{\beta}} \mathrm{d}\xi. \tag{14}$$

Given the simple expression of the trial functions, these integrals can be calculated analytically.

The kinetic energy of the y-wise stiffener on plate i is given by

$$T_y^i = (\dot{\mathbf{q}}^i)^{\mathrm{T}} \mathbf{M}_y^i \dot{\mathbf{q}}^i, \tag{15}$$

where $\mathbf{M}_y^i$ is the elementary mass matrix of the y-wise stiffener on plate i:

$$\begin{aligned}
\mathbf{M}_y^i &= [M_{ymnrs}^i] \\
&= \frac{2\rho_y^i b^i}{(a^i)^2} [S_y^i((\bar{z}^i)^2 + (\bar{x}^i)^2) + I_{zz}^i + I_{xx}^i] \phi_{m,\xi}(\xi_y)\phi_{r,\xi}(\xi_y) I_{ns}^{00} \\
&\quad + \frac{2\rho_y^i}{b^i} [S_y^i(\bar{z}^i)^2 + I_{xx}^i] \phi_m(\xi_y)\phi_r(\xi_y) I_{ns}^{11} \\
&\quad - \frac{\rho_y^i S_y^i \bar{x}^i b^i}{a^i} [\phi_{m,\xi}(\xi_y)\phi_r(\xi_y) + \phi_m(\xi_y)\phi_{r,\xi}(\xi_y)] I_{ns}^{00} \\
&\quad + \frac{\rho_y^i S_y^i b^i}{2} \phi_m(\xi_y)\phi_r(\xi_y) I_{ns}^{00}.
\end{aligned} \tag{16}$$

The strain energy of the x-wise stiffener on plate i is

$$V_y^i = (\mathbf{q}^i)^{\mathrm{T}} \mathbf{K}_y^i \mathbf{q}^i, \tag{17}$$

where $\mathbf{K}_y^i$ is the elementary stiffness matrix of y-wise stiffener on plate i:

$$\begin{aligned}
\mathbf{K}_y^i &= [K_{ymnrs}^i] \\
&= \frac{8E_y^i}{(b^i)^3} [I_{xx} + (\bar{z}^i)^2 S^i] \phi_m(\xi_y)\phi_r(\xi_y) I_{ns}^{22} \\
&\quad + \frac{8G_y^i}{(a^i)^2 b^i} J_y^i \phi_{m,\xi}(\xi_y)\phi_{r,\xi}(\xi_y) I_{ns}^{11}.
\end{aligned} \tag{18}$$

The corresponding expressions for the x-wise stiffener are obtained by permuting a and b, x and y as well as ξ and η. Again, the mass and stiffness matrices of the stiffeners can be calculated analytically.

Summing the elementary energy contributions over all the elements of the global structure allows the kinetic energy T and the strain energy V of the global structure to be written as

$$T = \dot{\mathbf{q}}^{\mathrm{T}} \mathbf{M} \dot{\mathbf{q}}, \qquad V = \mathbf{q}^{\mathrm{T}} \mathbf{K} \mathbf{q}, \tag{19, 20}$$

where $\mathbf{q} = \{\mathbf{q}^1; \mathbf{q}^2; \ldots; \mathbf{q}^i; \ldots; \mathbf{q}^{N_P}\}$ is the vector of the Rayleigh–Ritz coefficients for the assembly of the N_P plates and

$$\mathbf{M} = \begin{bmatrix} \mathbf{M}^1 & & & \\ & \ddots & \mathbf{0} & \\ & \mathbf{0} & \mathbf{M}^i & \\ & & & \mathbf{M}^{N_P} \end{bmatrix}, \qquad \mathbf{K} = \begin{bmatrix} \mathbf{K}^1 & & & \\ & \ddots & \mathbf{0} & \\ & \mathbf{0} & \mathbf{K}^i & \\ & & & \mathbf{K}^{N_P} \end{bmatrix} \tag{21}$$

are the global mass and stiffness matrices and

$$\mathbf{M}^i = \mathbf{M}_p^i + \mathbf{M}_x^i + \mathbf{M}_y^i, \qquad \mathbf{K}^i = \mathbf{K}_p^i + \mathbf{K}_x^i + \mathbf{K}_y^i \tag{22, 23}$$

are the elementary mass and stiffness matrices respectively. Application of the variational principle to the global structure leads to the eigenvalue problem

$$\mathbf{H}\mathbf{q} = \mathbf{0}, \tag{24}$$

where $\mathbf{H} = -\omega^2\mathbf{M} + \mathbf{K}$ and ω is the angular frequency.

3.3. FORCED RESPONSE

A plate element i can sustain external work W^i,

$$W^i = \frac{a^i b^i}{4} \int_{-1}^{+1} \int_{-1}^{+1} f^i(\xi^i, \eta^i) w^i(\xi^i, n^i)\, \mathrm{d}\xi^i\, \mathrm{d}\eta^i \tag{25}$$

or

$$W^i = (\mathbf{q}^i)^{\mathrm{T}} \mathbf{f}^i, \tag{26}$$

where $\mathbf{f}^i = \{f_{mn}^i\}$ is the elementary force vector on plate element i:

$$f_{mn}^i = \frac{a^i b^i}{4} \int_{-1}^{+1} f^i(\xi^i, \eta^i) \phi_m(\xi^i) \phi_n(\eta^i)\, \mathrm{d}\xi^i\, \mathrm{d}\eta^i. \tag{27}$$

$f^i(\xi^i, \eta^i)$ represents the transverse force per unit of area on element i. If the excitation is a point force at (ξ_0^i, η_0^i), $f^i(\xi^i, \eta^i) = f^i \delta(\xi^i - \xi_0^i)\delta(\eta^i - \eta_0^i)$, this leads to

$$f_{mn}^i = \frac{a^i b^i}{4} f^i(\xi_0^i, \eta_0^i) \phi_m(\xi_0^i) \phi_n(\eta_0^i). \tag{28}$$

The global force vector is $\mathbf{f} = \{\mathbf{f}^1; \mathbf{f}^2; \ldots; \mathbf{f}^i; \ldots\}$ and the forced response of the global structure is the solution of the linear system

$$(-\omega^2\mathbf{M} + \mathbf{K}) = \mathbf{f}. \tag{29}$$

4. INTER-ELEMENT CONDITIONS—CONDENSATION OF THE GLOBAL MASS AND STIFFNESS MATRICES

The global mass and stiffness matrices are obtained by assembling the previous elementary matrices. The continuity conditions at the interface between adjacent elements are now used to condense the global mass and stiffness matrices.

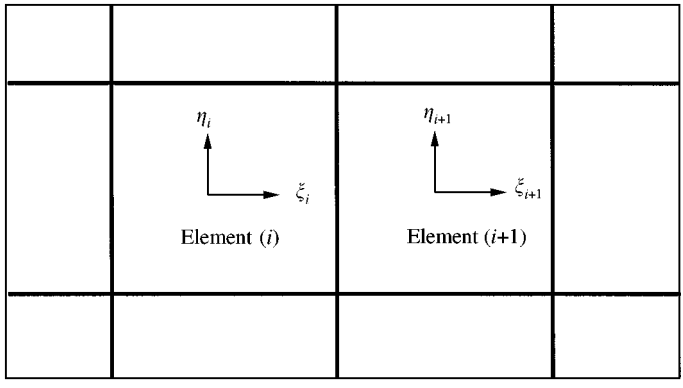

Figure 6. Illustration of the inter-element continuity.

Referring to Figure 6, the continuity between elements i and $i+1$ requires equality of the plate displacement and slope at the interface between elements i and $i+1$, for $-1 \leqslant \eta^i \leqslant +1$:

$$w^i(1, \eta^i) = w^{i+1}(-1, \eta^i), \tag{30}$$

$$\frac{2}{a^i}\frac{\mathrm{d}w^i(1, \eta^i)}{\mathrm{d}\xi^i} = \frac{2}{a^{i+1}}\frac{\mathrm{d}w^{i+1}(-1, \eta^i)}{\mathrm{d}\xi^{i+1}}. \tag{31}$$

Using the expansions of the displacements over the local trial functions,

$$\sum_{m=1}^{M}\sum_{n=1}^{N} q_{mn}^i \phi_m(1)\phi_n(\eta^i) = \sum_{m=1}^{M}\sum_{n=1}^{N} q_{mn}^{i+1}\phi_m(-1)\phi_n(\eta^i), \tag{32}$$

$$\sum_{m=1}^{M}\sum_{n=1}^{N} q_{mn}^i \frac{\mathrm{d}\phi_m}{\mathrm{d}\xi}(1)\phi_n(\eta^i) = \frac{a^i}{a^{i+1}}\sum_{m=1}^{M}\sum_{n=1}^{N} q_{mn}^{i+1}\frac{\mathrm{d}\phi_m}{\mathrm{d}\xi}(-1)\phi_n(\eta^i). \tag{33}$$

Here, the values of the trigonometric trial functions at the end points -1 and $+1$ are used to simplify the above expressions. Using the results of Figure 5, we note that

$$\phi_m(1)\begin{cases} = 1 \text{ for } m = 3, \\ = 0 \text{ otherwise}, \end{cases} \qquad \phi_m(-1)\begin{cases} = 1 \text{ for } m = 1, \\ = 0 \text{ otherwise}, \end{cases} \tag{34}$$

$$\frac{\mathrm{d}\phi_m}{\mathrm{d}\xi}(1)\begin{cases} = \frac{\pi}{2} \text{ for } m = 4, \\ = 0 \text{ otherwise}, \end{cases} \qquad \frac{\mathrm{d}\phi_m}{\mathrm{d}\xi}(-1)\begin{cases} = \frac{\pi}{2} \text{ for } m = 2, \\ = 0 \text{ otherwise}. \end{cases} \tag{35}$$

Hence, the displacement and slope continuity conditions become

$$\sum_{n=1}^{N} q_{3n}^i \phi_n(\eta^i) = \sum_{n=1}^{N} q_{1n}^{i+1}\phi_n(\eta^i), \tag{36}$$

$$\frac{\pi}{2}\sum_{n=1}^{N} q_{4n}^i \phi_n(\eta^i) = \frac{\pi}{2}\frac{a^i}{a^{i+1}}\sum_{n=1}^{N} q_{2n}^{i+1}\phi_n(\eta^i). \tag{37}$$

Since the functions $\phi_n(\eta^i)$ form a basis on $-1 \leqslant \eta^i \leqslant +1$, the above equalities reduce to

$$q^i_{3n} = q^{i+1}_{1n}, \qquad q^i_{4n} = \frac{a_i}{a_{i+1}} q^{i+1}_{2n}. \tag{38, 39}$$

for $1 \leqslant n \leqslant N$. Alternatively, if elements i and $i+1$ have an interface parallel to the x-axis, the continuity of the plate displacement and slope requires

$$w^i(\xi^i, 1) = w^{i+1}(\xi^i, -1), \tag{40}$$

$$\frac{2}{b^i}\frac{\mathrm{d}w^i(\xi^i, 1)}{\mathrm{d}\eta^i} = \frac{2}{b^{i+1}}\frac{\mathrm{d}w^{i+1}(\xi^i, -1)}{\mathrm{d}\eta^{i+1}}. \tag{41}$$

This lead to the conditions

$$q^i_{m3} = q^{i+1}_{m1}, \qquad q^i_{m4} = \frac{b_i}{b_{i+1}} q^{i+1}_{m2} \tag{42, 43}$$

for $1 \leqslant m \leqslant M$. Thus, due to the properties of the proposed trigonometric functions at the end points -1 and $+1$, the displacement and slope continuity at the interface of adjacent elements translate into simple conditions on the unknown Rayleigh–Ritz coefficients of adjacent elements. These conditions allow the global eigenvalue problem to be condensed by eliminating the redundant Rayleigh–Ritz coefficients. The condensation procedure is briefly explained in what follows.

In order to simplify the notations and the presentation, we temporarily denote $\mathbf{q} = \{q_1; \ldots; q_f; \ldots; q_g; \ldots\}$ the vector of the Rayleigh–Ritz coefficients of the assembly, and we consider a continuity condition of the general form

$$q_g = \alpha q_f, \tag{44}$$

like in equations (38) and (42). This condition allows the two dependent degrees of freedom q_f and q_g to be condensed into a single degree of freedom, e.g., q_f. Before imposing the above condition, the eigenvalue problem takes the form

$$\mathbf{Hq} = \mathbf{0} \tag{45}$$

or

$$\begin{bmatrix} H_{11} & \cdots & H_{f1} & \cdots & H_{g1} & \cdots \\ \vdots & & \vdots & & \vdots & \\ H_{1f} & \cdots & H_{ff} & \cdots & H_{gf} & \cdots \\ \vdots & & \vdots & & \vdots & \\ H_{1f} & \cdots & H_{fg} & \cdots & H_{gg} & \cdots \\ \vdots & & \vdots & & \vdots & \end{bmatrix} \begin{Bmatrix} q_1 \\ \vdots \\ q_f \\ \vdots \\ q_g \\ \vdots \end{Bmatrix} = \mathbf{0}. \tag{46}$$

The Hamilton functional takes the form

$$H = \sum_i \sum_j q_i H_{ij} q_j. \tag{47}$$

This expression can be modified to isolate the redundant degree of freedom q_g,

$$H = \sum_{i \neq g} \sum_{j \neq g} q_i q_j H_{ij} + \sum_{i \neq g} q_i H_{ig} q_g + \sum_{j \neq g} q_g H_{gj} q_j + q_g H_{gg} q_g. \tag{48}$$

Inserting the condition $q_g = \alpha q_f$,

$$H = \sum_{i \neq g} \sum_{j \neq g} q_i H_{ij} q_j + \sum_{i \neq g} \alpha q_i H_{ig} q_f + \sum_{j \neq g} \alpha q_f H_{gj} q_j + \alpha^2 q_f H_{gg} q_f. \tag{49}$$

Setting $\partial H / \partial qk$ for all k yields the condensed system where the degree of freedom q_g is now eliminated,

$$\begin{bmatrix} H_{11} & \cdots & H_{f1} + \alpha H_{g1} & \cdots \\ \vdots & & \vdots & \\ H_{1f} + \alpha H_{1g} & \cdots & H_{ff} + \alpha H_{gf} + \alpha H_{fg} + \alpha^2 H_{gg} & \cdots \\ \vdots & & \vdots & \end{bmatrix} \begin{Bmatrix} q_1 \\ \vdots \\ q_f \\ \vdots \end{Bmatrix} = \mathbf{0}. \tag{50}$$

Thus, the condensation consists of linearly combining the rows and columns associated to the dependent degrees of freedom. This procedure is repeated for all the dependent degrees of freedom, as obtained from the inter-element continuity conditions. The condensed eigenvalue problem is then solved for the eigenfrequencies and mode shapes of the global structure.

5. NUMERICAL RESULTS FOR A HOMOGENEOUS PLATE

In a first instance, the method has been applied to a homogeneous (non-stiffened) plate in order to test the convergence properties of the method. The non-stiffened plate is simply a particular case where all stiffener energies are set to zero. A square, homogeneous, rectangular plate of dimensions $1{\cdot}2\,\mathrm{m} \times 1{\cdot}0\,\mathrm{m}$, thickness $2{\cdot}5\,\mathrm{mm}$, made of steel material ($E = 200\,\mathrm{GPa}$, $\rho = 7800\,\mathrm{kg/m^3}$, $\nu = 0{\cdot}3$) has been considered in these simulations. The plate is simply supported, so that the calculated eigenfrequencies can be compared to the exact solutions, $f_{ij} = 1/2\pi\sqrt{(D/\rho h)}[(i\pi/a)^2 + (j\pi/b)^2]$, where i, j are mode indices. Simply supported boundary conditions are realized by removing in the Rayleigh–Ritz expansion the hierarchical trigonometric functions which take a non-zero value on the plate edges. In the context of hierarchical finite elements, two discretization parameters need to be considered: the size of the elements, and the degree of the interpolation functions over each element. In this simulation, the plate was meshed using the various configurations shown in Figure 7 (either 1×1, 2×1, 2×2 or 4×4 plate elements), and a variable number of hierarchical trigonometric functions was considered over each element. Of interest here is whether large elements with many local hierarchical functions, or small elements with few local hierarchical functions, are preferable.

Table 2 shows the results obtained for the various configurations; the second column gives the number of hierarchical functions used on each element, the third column gives the total number of degrees of freedom (d.o.f.) of the system after imposing the boundary conditions and the inter-element conditions, and the last two columns give the number of eigenfrequencies calculated with an error less than 1% and less than 2% with respect to the exact eigenfrequencies respectively. These results show that, for a given total number of d.o.f. the number of eigenfrequencies calculated with a given accuracy is in most cases larger

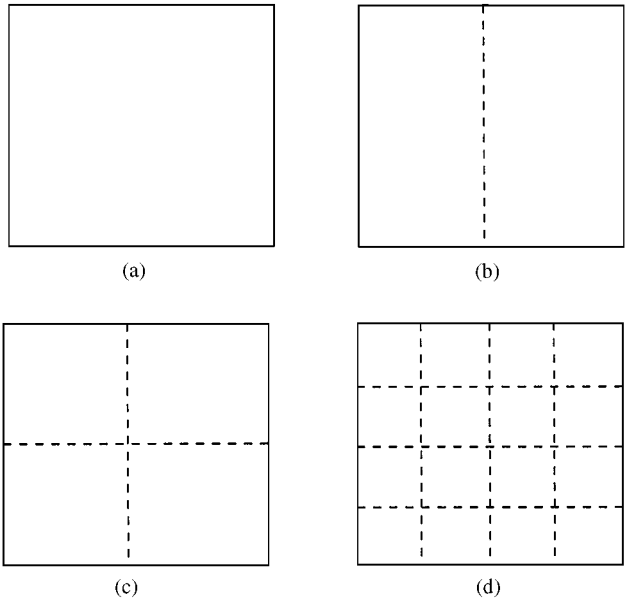

Figure 7. Various meshes for a homogeneous, simply supported plate: (a) 1×1 element, (b) 2×1 elements, (c) 2×2 elements, (d) 4×4 elements.

TABLE 2

Results for a homogeneous, simply supported plate

Mesh	$M_i \times N_i$	d.o.f.	No. of modes within 1% error	No. of modes within 2% error
1×1	14×14	144	45	45
2×1	8×14	144	35	58
2×2	8×8	144	35	58
4×4	5×5	144	0	0
1×1	34×34	1024	527	629
2×1	18×34	1024	439	593
2×2	18×18	1024	430	586
4×4	10×10	1024	249	505
1×1	50×50	2304	1423	1502
2×1	26×50	2304	1369	1451
2×2	26×26	2304	1203	1441
4×4	14×14	2304	953	1300
1×1	62×62	3600	2312	2418
2×1	32×62	3600	2210	2340
2×2	32×32	3600	2210	2311
4×4	17×17	3600	1884	2127

when large elements and many hierarchical functions are considered, instead of small elements and few hierarchical functions.

Figure 8 shows the number of modes calculated within a 2% error, as a function of the number of d.o.f. for three different meshes: 1×1, 2×1, 2×2 and 4×4 elements. This plot

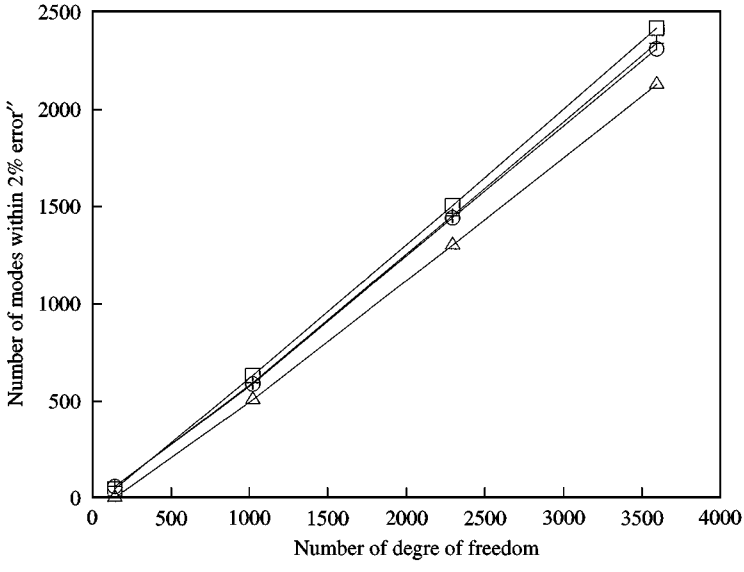

Figure 8. Convergence of the method for a homogeneous, simply supported plate. Numbers of modes within 2% error for 1×1 mesh (□); 2×1 mesh (+); 2×2 mesh (○); 4×4 mesh (△).

shows that, again, a coarser mesh with a larger number of local functions is preferable for more accurate results. Additionally, the relation between the number of modes within a 2% error and the number of d.o.f. is almost linear. This is in fact consistent with the requirement that enough test functions should be used with regard to the smallest structural wavelength to be observed in the plate. If one defines the structural wavelength λ at the frequency f,

$$\lambda = \sqrt{2\pi}\left(\frac{D}{\rho h}\right)^{1/4} f^{-1/2}, \tag{51}$$

then the number of test functions N^i used in a given direction at the frequency f must be a constant times the number of wavelengths to be observed along the corresponding dimension of the element, a/λ. It was found that a value of 3 times the number of wavelengths a/λ is sufficient to guarantee the convergence within a 2% error.

6. NUMERICAL RESULTS FOR STIFFENED PLATES

6.1. CONVERGENCE STUDY

The same simply supported plate as in section 5 is considered, with a y-wise stiffener passing through the center of the plate. The stiffener has a rectangular cross-section with height 20 mm and width 10 mm and the same material characteristics as the plate. Various meshes represented in Figure 7 were also considered, with a variable number of hierarchical trigonometric functions over each element.

In each case, the stiffener was positioned at the edge of one element except for the 1×1 mesh where the stiffener was located at the center of the element by setting $\xi_s = 0$ in equations (16) and (18).

The numerical results are shown in the Table 3. The results show that the number of converged modes in the stiffened and unstiffened cases are comparable in the various

TABLE 3

Results for a stiffened simply supported plate; a 2×1 *mesh with* 4352 *d.o.f. was used to compute the "exact" solution for the stiffened plate*

Mesh	$M_i \times N_i$	d.o.f.	No. of modes within 1% error	(unstiffened)	No. of modes within 2% error	(unstiffened)
1×1	14×14	144	1	(45)	2	(45)
2×1	14×8	144	15	(35)	52	(58)
2×2	8×8	144	15	(35)	52	(58)
4×4	5×5	144	0	(0)	0	(0)
1×1	34×34	1024	8	(527)	176	(629)
2×1	34×18	1024	399	(439)	574	(593)
2×2	18×18	1024	399	(430)	574	(586)
4×4	10×10	1024	235	(249)	481	(505)
1×1	50×50	2304	95	(1423)	1406	(1502)
2×1	50×26	2304	1150	(1369)	1424	(1451)
2×2	26×26	2304	1150	(1203)	1424	(1441)
4×4	14×14	2304	835	(953)	1274	(1300)

configurations. Also, coarser meshes with a large number of interpolation functions are preferable to refined meshes with few interpolation functions, as in the case of the unstiffened plate.

When the stiffener is placed between two elements (2×1, 2×2, 4×4 meshes), the number of converged modes is comparable to the number of modes without stiffener. Therefore, the rules to determine the number of functions needed is similar in the unstiffened and stiffened cases.

There are convergence problems with the 1×1 mesh. This is due to the inability of global functions to reconstruct the local modes of the stiffened plates. When heavy stiffeners are considered, most of the modes are local and the transverse displacement is small at the stiffener location. The global functions are not necessarily null at the stiffener location and this leads to poor convergence. Imposing the stiffener to be at the interface between two elements allows local modes to be more easily reconstructed.

6.2. COMPARISON WITH THE LITERATURE

There are no exact solutions of the eigenfrequencies of finite, stiffened rectangular plates. Therefore, comparisons of the present method with other numerical results reported in the literature are presented in this section. Koko *et al.* [15] have presented simulations of the free vibration of stiffened plates using the so-called "super-elements"; plate and beam super-elements were developed by these authors in order to model the free vibration of stiffened plates.

In Koko's work, the plate element accounts for both in-plane and transverse displacements. Each element has 55 variables and displacements are represented by analytical and polynomial functions. A mix of quadratic Lagrange polynomials, cubic Hermitian polynomials and trigonometric (sine) functions are used as interpolation functions. In addition to the in-plane and out-of-plane bending displacement, torsional

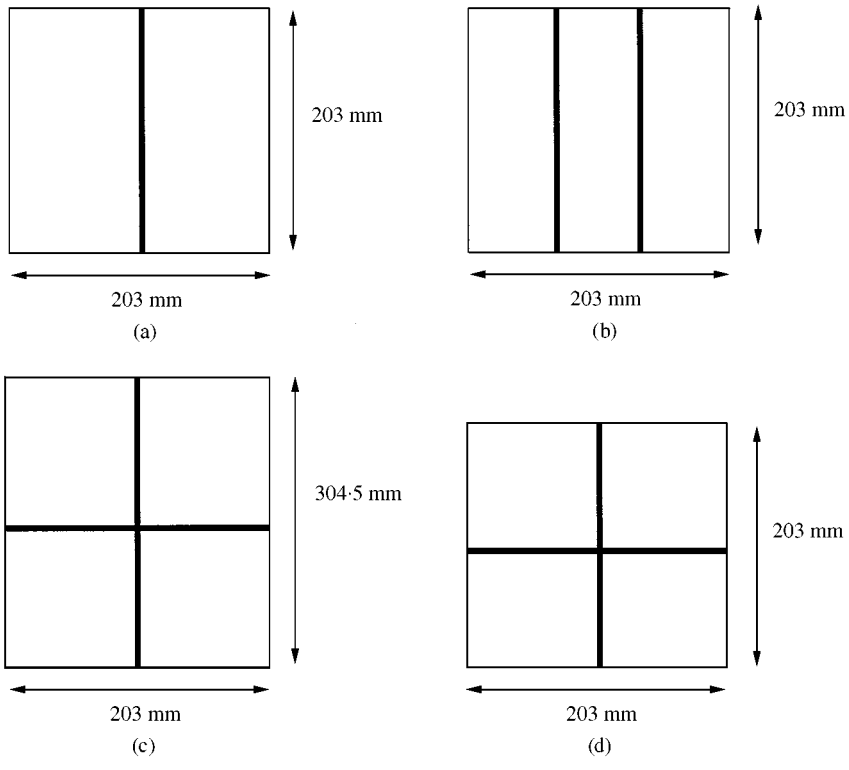

Figure 9. Configuration of stiffened plates for comparisons with Koko *et al.* [15]: (a) case 1, (b) case 2, (c) case 3, (d) case 4.

rotation and lateral bending displacement are also included in the beam element. The beam element has 18 variables.

A fundamental modelling difference with the present theory is that Koko *et al.* [15] allow for in-plane displacements of the plate, whereas the present theory assumes pure bending deformation of the plate; however, such effects are expected to be small for thin plates. Plate super-elements generally correspond to the domain comprised between adjacent stiffeners (Type I mesh); in some cases, Koko *et al.* use 2×2 super-elements to model these inter-stiffener domains (Type II mesh).

The comparisons presented hereafter correspond to the structural configurations shown in Figure 9. In all cases, the plate is clamped on its four sides; in the context of the hierarchical trigonometric functions, the case of a clamped plate is realized by removing in the Rayleigh–Ritz expansion those functions whose value or first derivative value is zero on the plate edges. For case 1, the plate has a thickness $h = 1{\cdot}27$ mm, the plate and stiffeners material characteristics are $E = 68{\cdot}9$ GPa, $\rho = 2670\,\text{kg/m}^3$, $\nu = 0{\cdot}3$, and two different stiffener sections are considered: either a "full" stiffener (rectangular cross-section with height 11·33 mm and width 6·35 mm), or a "reduced" stiffener (rectangular cross-section with height 8·28 mm and width 4·93 mm).

For case 2, the plate characteristics are the same but two different stiffener sections are considered: either a "full" stiffener (rectangular cross-section with height 16·53 mm and width 2·29 mm), or a "reduced" stiffener (rectangular cross-section with height 11·43 mm and width 1·85 mm).

TABLE 4

Eigenfrequencies for case 1

		Natural frequencies (Hz)				
Stiffener	Mode	Unstiffened	Present	Koko [15]	FE [15]	Experiment [15]
Full rib	1	292.8	727.8	736.8	718.1	689.0
	2	597.2	783.2	769.4	751.4	725.0
	3	597.6	1015.5	1019.6	997.4	961.0
	4	881.3	1033.8	1032.3	1007.1	986.0
	5	1071.3	1450.0	1483.7	1419.8	1376.0
	6	1076.6	1457.9	1488.3	1424.3	1413.0
Reduced rib	1	292.8	671.2	679.1	670.7	627.0
	2	597.2	744.4	716.9	724.0	662.0
	3	597.6	984.6	990.1	977.2	924.0
	4	881.3	1027.2	1022.9	1002.1	953.0
	5	1071.3	1434.4	1469.3	1408.7	1370.0
	6	1076.5	1451.9	1442.3	1414.1	1338.0

TABLE 5

Eigenfrequencies for case 2

		Natural frequencies (Hz)				
Stiffener	Mode	Unstiffened	Present	Koko [15]	FE [15]	Experiment [15]
Full rib	1	271.4	949.3	1072.8	965.3	909.0
	2	553.6	1265.8	1334.2	1272.3	1204.0
	3	554.0	1331.8	1410.3	1364.3	1319.0
	4	816.9	1464.0	1483.2	1418.1	1506.0
	5	993.0	1572.7	1649.2	1602.9	1560.0
	6	997.9	1739.9	1730.5	1757.1	1693.0
Reduced rib	1	271.4	923.6	938.5	928.6	859.0
	2	553.6	1202.4	1178.6	1205.1	1044.0
	3	554.0	1236.1	1182.4	1229.8	1292.0
	4	816.9	1264.7	1330.4	1274.6	1223.0
	5	993.0	1540.5	1569.8	1557.4	1503.0
	6	997.9	1696.9	1674.5	1714.5	1650.0

For cases 3 and 4, the plate has a thickness 1·37 mm, the plate and stiffeners material characteristics are $E = 71\,\text{GPa}$, $\rho = 2700\,\text{kg/m}^3$, $\nu = 0{\cdot}3$, and the stiffeners have a rectangular cross-section with height 11·3 mm and width 6·35 mm.

Koko *et al.* [15] have also reported experimental values of the natural frequencies in the above configurations, as well as the natural frequencies obtained from finite element calculations. Tables 4–6 show the eigenfrequencies obtained from the various methods.

The agreement of the present approach with the numerical and experimental results reported by reference [15] is good.

TABLE 6

Eigenfrequencies for case 3

Mode	Unstiffened	Present	Koko mesh I	Koko mesh II
1	221.8	828.4	846.8	838.2
2	342.5	832.5	846.1	841.6
3	543.0	851.8	849.4	844.2
4	546.4	862.3	862.0	858.4
5	655.4	1298.9	1448.0	1254.3
6	828.2	1336.4		1354.6
7	847.1	1344.0		1347.3
8	1029.1	1352.5		1353.6
9	1118.0	1596.1		1503.0

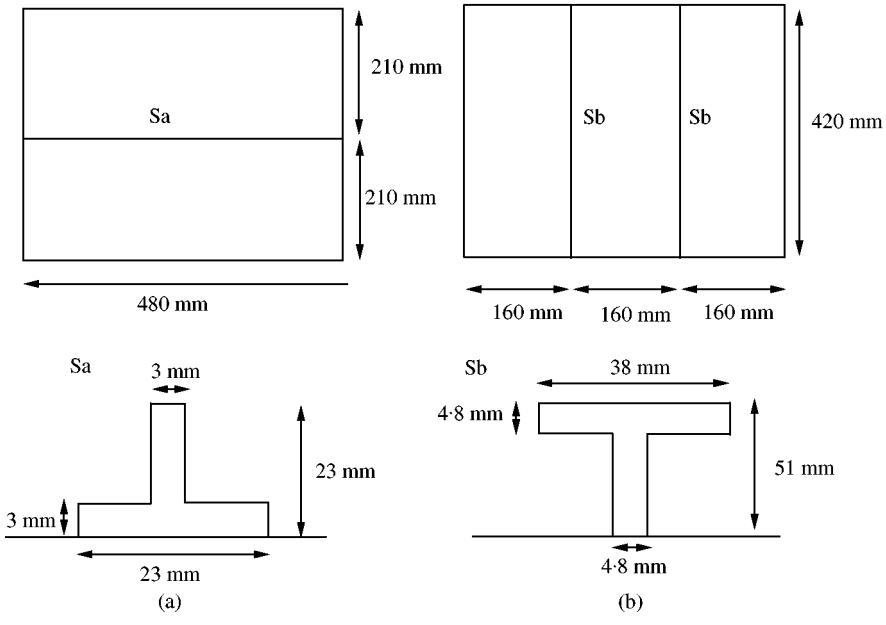

Figure 10. Configurations of the experimental stiffened plates: (a) case 1, (b) case 2.

6.3. COMPARISON WITH EXPERIMENTAL RESULTS

Experiments have been conducted to measure the response of stiffened plates under a point-force excitation. The experimental configurations are shown in Figure 10. A base plate of dimensions 480 mm × 420 mm, thickness 3·22 mm, made of aluminum ($E = 68{\cdot}5$ GPa, $\rho = 2680\,\text{kg/m}^3$, $\nu = 0{\cdot}33$) was considered, with two different stiffener configurations: either one widthwise stiffener (case 1) or two widthwise stiffeners (case 2); the stiffeners were cut in standard "T" sections as shown in Figure 10 and bonded to the plate. The material characteristics of the stiffeners are identical to those of the plate.

The plate was supported on strips of thin shim spring steel, one end of which was mounted along the plate edges in a direction perpendicular to the plate surface; the other

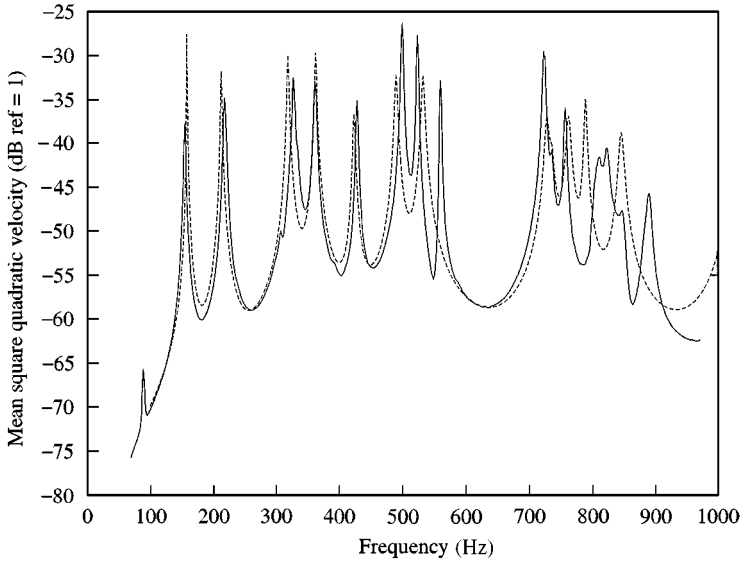

Figure 11. Comparison with the experimental results for case 1 (1 stiffener): —, experimental result; - - -, numerical result.

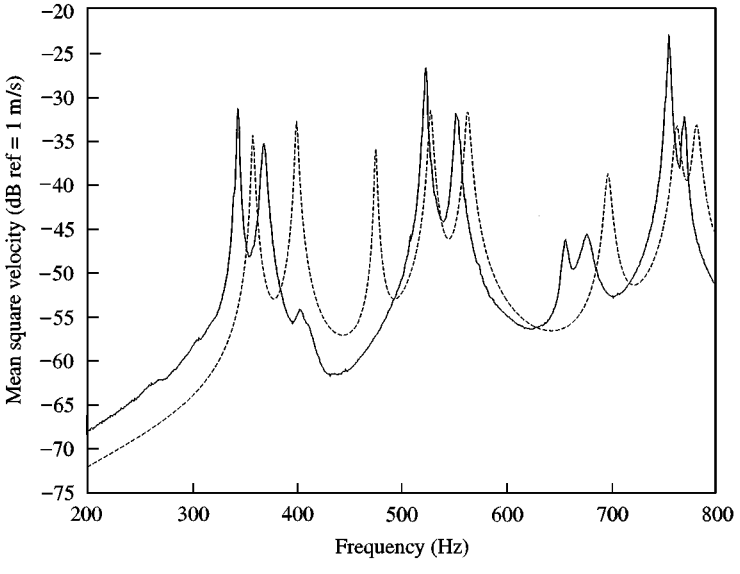

Figure 12. Comparison with the experimental results for case 2 (2 stiffeners): —, experimental result; - - -, numerical result.

end of the strips was fixed into a rigid frame. Such supports have been shown to correctly approximate simply supported boundary conditions [21]. The stiffened plates were excited by a shaker on which a stinger was mounted to approximate a transverse point-force excitation; the shaker was fed by a pseudo-random noise in the 0–800 Hz frequency range. The excitation point was located at $x = 80$ mm, $y = 70$ mm from a plate corner in all cases. The magnitude F of the excitation force was measured, together with the magnitude of the

TABLE 7

Eigenfrequencies for case 4

Mode	Unstiffened	Present	Koko mesh I	Koko mesh II
1	295.5	1135.3	1149.6	1141.7
2	602.7	1153.0	1152.5	1148.0
3	602.7	1153.0	1161.9	1157.4
4	888.8	1153.0	1161.9	1157.4
5	1080.7	2021.9	2042.1	1859.8
6	1085.8	2328.1		2348.0
7	1355.3	2328.5		2342.1
8	1355.3	2328.5		2342.1
9	1729.5	2330.0		2390.1

transverse velocity V_i, using a Doppler laser vibrometer. The panel is discretized into $n = 361\,(19 \times 19)$ measurement points regularly spaced on the vibrating surface. The response was then calculated in terms of the mean-square admittance of the structure,

$$10 \log_{10} \frac{\sum_{i=1}^{n} V_i^2}{2nF^2}. \tag{52}$$

Figures 11 and 12 show the comparisons between the experiments and the simulations for cases 1 and 2 respectively. The simulation results have been obtained with one element between consecutive stiffeners and 20×15 hierarchical functions over each element.

The agreement between the theory and the experiment is generally very good in case 1, up to 500 Hz. There are more deviations in case 2, which corresponds to a much more stiffening configuration than case 1. In general, the theory over-estimates the experimental resonance frequencies in case 2; it is suspected that the actual junction conditions between the stiffeners and the plate do not respect some of the theoretical continuity conditions (such as the rotation continuity).

7. CONCLUSION

The vibration analysis of stiffened plates using hierarchical finite elements with a set of trigonometric interpolation functions has been presented. The comparison of the present approach with the literature and experimental results show good agreement. It was found that, in general, more accurate results are obtained when using few discretization elements and high order interpolation functions. The trigonometric functions naturally reproduce free vibration shapes of plate elements comprised between stiffeners, which leads to well-conditioned systems and the possibility of accurately calculating a large number of vibration modes. This great numerical stability of the trigonometric functions and their readiness for symbolic manipulations make them potentially attractive for vibration and should radiation analysis in the mid-frequency range.

REFERENCES

1. J.-R. WU and W. LIU 1988 *Journal of Sound and Vibration* **123**, 103–113. Vibration of rectangular plates with edge restraints and intermediate stiffeners.

2. P. A. A. LAURA and R. GUTIERREZ 1981 *Journal of Sound and Vibration* **78**, 139–144. A note on transverse vibration of stiffened rectangular plates with edges elastically restrained against rotation.
3. R. BHAT 1985 *Journal of Sound and Vibration* **102**, 493–499. Natural frequencies of rectangular plates using characteristic orthogonal polynomials in rayleigh-ritz methods.
4. R. GUTIERREZ and P. A. A. LAURA 1985 *Journal of Sound and Vibration* **101**, 122–124. Transverse vibration of rectangular plates elastically restrained against rotation along the edges.
5. K. LIEW, Y. XIANG, S. KITIPORNCHAI and M. LIM 1994 *Journal of Vibration and Acoustic* **166**, 529–535. Vibration of the rectangular mindlin plates with intermediate stiffeners.
6. K. LIEW, Y. XIANG, S. KITIPORNCHAI and J. MEEK 1995 *Comput. Methods Appl. Mech. Eng* **120**, 339–353. Formulation of mindlinengesser model for stiffened plate vibration.
7. Y. XIANG, S. KITIPORNCHAI, K. LIEW and M. LIM 1995 *Acta Mechanica* **112**, 11–18. Vibration of stiffened skew mindlin plates.
8. A. BERRY and J. NICOLAS 1996 *Journal of Acoustical Societies of America* **100**, 312–319. Vibration and sound radiation of fluid-loaded stiffend plates with consideration of in-plane deformation.
9. H. MOLAGHASEMI and I. HARIK 1996 *Journal of Sound and Vibration* **190**, 726–732. Free vibration of stiffened sector plates.
10. B. MACE 1980 *Journal of Sound and Vibration* **73**, 473–486. Periodically stiffened fluid-loaded plates, I: response to convected harmonic pressure and free wave propagation.
11. B. MACE 1980 *Journal of Sound and Vibration* **73**, 487–504. Periodically stiffened fluid-loaded plates, II: response to line and point forces.
12. B. MACE 1981 *Journal of Sound and Vibration* **79**, 439–452. Sound radiation from fluid loaded orthogonally stiffened plates.
13. D. MEAD 1990 *Journal of Acoustical Societies of America* **88**, 391–401. Plates with regular stiffening in acoustic media: vibration and radiation.
14. A. BERRY and J. NICOLAS 1994 *Applied Acoustics* **100**, 185–215. Structural acoustics and vibration behavior of complex panels.
15. T. KOKO and M. OLSON 1992 *Journal of Acoustical Societies of America* **158**, 149–167. Vibration analysis of stiffened plates by super elements.
16. C. CHEN, W. LIU and S. CHERN 1994 *Computer & Structure* **50**, 471–480. Vibration analysis of stiffened plates.
17. A. COTÉ 1998 *Ph.D. thesis, Université de Sherbrooke.* Modélisation vibroacoustique dans le domaine des moyennes fréquences par éléments finis de type P.
18. D. MEAD, D. ZHU and N. BARDELL 1988 *Journal of Sound and Vibration* **127**, 19–48. Free vibration of an orthogonally stiffened flat plate.
19. D. MEAD, D. ZHU and N. BARDELL 1991 *Journal of Sound and Vibration* **151**, 262–289. Free vibration analysis of flat plate using the hierarchical finite element method.
20. O. BESLIN and J. NICOLAS 1996 *Journal of Acoustical Societies of America.* A hierarchical functions set for predicting very high order plate bending modes with any boundary conditions.
21. Y. CHAMPOUX, S. BRUNET and A. BERRY 1996 *Experimental Techniques* **158**, 149–167. On the construction of a simply supported rectangular plate for noise and vibration studies.